Adhesion enhancement and damage protection for carbon fiber-reinforced polymer (CFRP) composites via silica particle coating

Kyungtae Kim[a,b], Yong Chae Jung[a], Seong Yun Kim[c,*], B.J. Yang[a,*], Jaewoo Kim[a,*]

[a] *Institute of Advanced Composite Materials, Korea Institute of Science and Technology (KIST), 92, Chudong-ro, Bongdong-eup, Wanju-gun, Jeollabuk-do 55324, Republic of Korea*
[b] *Defense Venture Department, Defense Agency for Technology and Quality (DTaQ), 420, Dongjin-ro, Jinju-si, Gyeongsangnam-do 52851, Republic of Korea*
[c] *Chonbuk National University, 567, Baekje-daero, Deokjin-gu, Jeonju-si, Jeollabuk-do 54896, Republic of Korea*

ARTICLE INFO

ABSTRACT

Adhesive materials for carbon fiber reinforced polymer (CFRP) composites have attracted the interest of researchers as an effective means to bond newly developed lightweight and high-performance composite structures. In this study, we developed a novel method to overcome these critical problems through a silica particle coating. Four-step bonding procedures were proposed to bind heterogeneous materials, where various concentrations of silica particles were introduced to coat CFRP composite surfaces uniformly in order to serve as a reinforcement and as a protection barrier layer against CFRP fractures. Experimental evaluations of the mechanics and fractography studies were conducted to clarify the correlations among the silica concentrations, adhesive strength levels, coating properties, and CFRP surface fractures. It was demonstrated that the introduction of the silica surface coating improves the adhesive strength by approximately 20% while also reducing CFRP surface fractures significantly by around 90%.

1. Introduction

Carbon fiber reinforced polymer (CFRP) composites have excellent engineering properties, such as a high strength-to-weight ratio, good impact resistance, and non-corrosive characteristics, thus attracting much attention in a wide variety of fields that require high strength and lightweight properties [1]. The annual demand for CFRP composites has been steadily increasing, especially in the aircraft and aerospace industries, where lightweight materials are in dire need. For example, up to 50% of the original weight was replaced by CFRP composite materials in the Boeing 787 airplane, and the proportion of CFRP parts is increasing in the automobile industry in order to maximize fuel efficiency [2,3]. Although the cost of CFRP composites remains a major obstacle, it will gradually decrease with the help of manufacturing techniques; therefore, the CFRP composite market is expected to prosper in the near future [4].

In order for CFRPs to be more commonly used in future markets, it is crucial to join CFRP composites with different materials, such as aluminum (Al), iron, and certain ceramics [5–7]. Traditionally the most commonly used joining methods were welding and bolting, but these methods cannot be applied to CFRP composites. Welding does not apply to polymeric materials or composites, and bolting causes irreversible damage to the structural integrity of CFRP composites [8,9]. Furthermore, bolting inevitably raises the overall weight due to the added bolts and nuts. In order to overcome these problems, adhesive bonding methods have been widely studied, as this approach can achieve high bonding strength levels, easy processability and a weight reduction at the same time [10].

Hence, intensive research has been carried to assess various types of adhesives and modifications of these adhesives, as summarized in Table 1. Particularly, in order to improve the performance of an adhesive, it is common to modify the epoxy with carbon nanotube (CNT) or silica nanoparticles as a filler material [11–14]. Korayem et al. proposed the incorporation of carbon nanotube (CNT) into an epoxy adhesive to increase the crosslinking density and to provide reinforcement effects, resulting in good crack growth inhibition when using the epoxy adhesive [15]. Another report about the addition of CNT to an epoxy material revealed that the adhesive strength increased by approximately 10% with a tensile modulus as high as 30% [16]. As another type of filler, silica was introduced to enhance the adhesive strength, by 38%, and the environmental effects like moisture and temperature conditions were observed as well [17].

The adhesive strength can also be enhanced by cleaning or increasing the adhesive surface area. IR and UV laser methods have been

---

Table 1
Adhesive bonding studies using various pre-treatment.

| Pre-treatment		Effect		Increase in adhesive strength	Ref.
Filler	Carbon nanotube (CNT)	Prevent cracking from epoxy matrix		50%	[15]
				10%	[16]
	Silica			38%	[17]
IR/UV laser		Clean or increase contact surface	Remove pollutants on adhesive surface	–	[18] [19]
CO_2 laser				78.8%	[20]
Nd:YAG laser			Increase surface area through pattern or structure formation	–	[21]
Vapor pressurized plasma				–	[22]
Homogeneous low-energy electron beam irradiation (HLEBI)		Increase binding energy between the metal and polymer		29%	[23]
Ultrasonic vibration		Allow adhesive to penetrate into the contact surface structure		52%	[24]
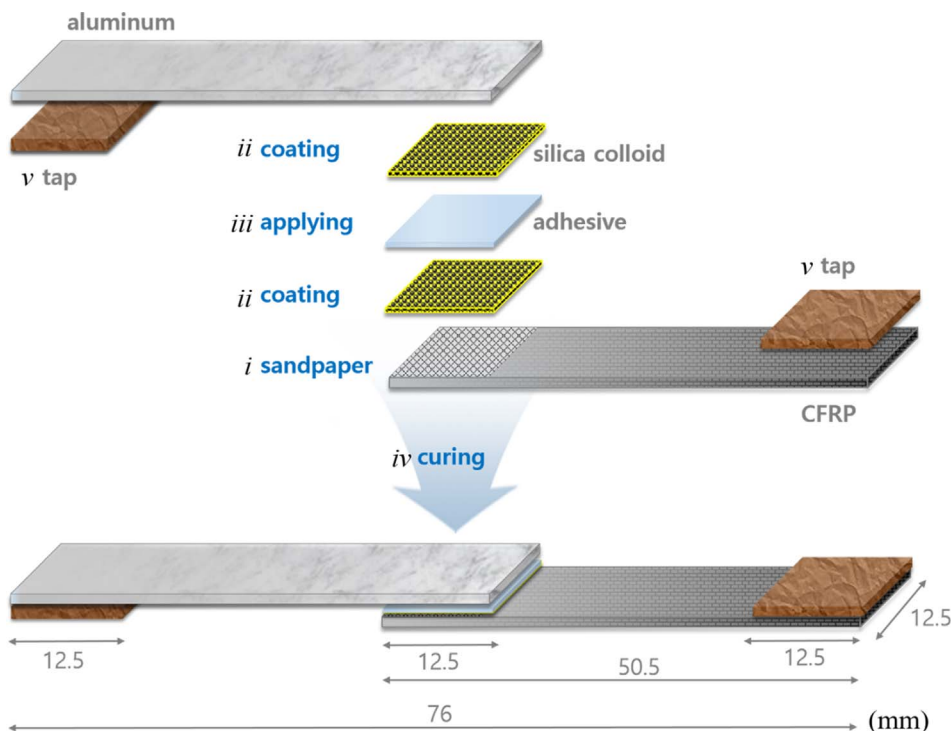
Fig. 1. Specimen fabrication sequence of the silica-coated CFRP/Al specimen preparation process for the lap shear test: *i.* Sandpaper to roughen the contact surface, *ii.* Drop-coat colloidal silica, *iii.* Apply adhesive onto the silica-coated surface, *iv.* Fix CFRP/Al with adhesive by a clamp and follow subsequent curing steps, *v.* Tap specimens by sandpaper.

Table 2
Details of the adhesives and curing conditions.

Products	Type	Ingredient	Thickness (mm)	Curing conditions
Araldite 2011-A/B	Paste	epoxy	≤ 0.1	150 °C for 30 min + 180 °C for 10 min
LF-501	Film			175 °C for 20 min + 200 °C for 10 min

used to remove contaminants from adhesion sites to maximize the surface activity [18,19]. When the surface was treated with a CO_2 laser, a 78% improvement in the adhesive strength was reported [20]. The nanosecond pulsed Nd:YAG laser method was been applied to modify the surface microstructure without damaging embedded carbon fibers [21]. A vapor-pressurized plasma treatment which can form a nano-pattern topography on the material surface was also applied to roughen the adhesion surface [22]. The advantages of these laser and plasma processing techniques are that they are clean, stable, rapid, and reproducible. In other approaches, enhanced binding energy between a metal and a polymer was achieved via a homogeneous low energy electron beam irradiation (HLEBI) method, and the adhesive strength was increased by 29% [23]. It was also reported that ultrasonic vibration enables an adhesive to penetrate the surface roughness of the bonding area, thus increasing the effective bonding area and improving the adhesive strength, by 52% in one study [24].

Given all of these research outcomes and the continuing efforts to enhance the adhesive strength, there is another critical problem to overcome before more widespread use of these materials can be realized. This is the damage commonly caused to CFRP composite materials during the debonding process [25–28]. When CFRP composites are debonded from other materials, fractures usually occur inside the CFRP, as the adhesive force surpasses the structure integrity of the CFRP itself. These damaged CFRP composites are generally buried [29,30] and/or recycled by the burning or melting of the matrix polymer to regain the
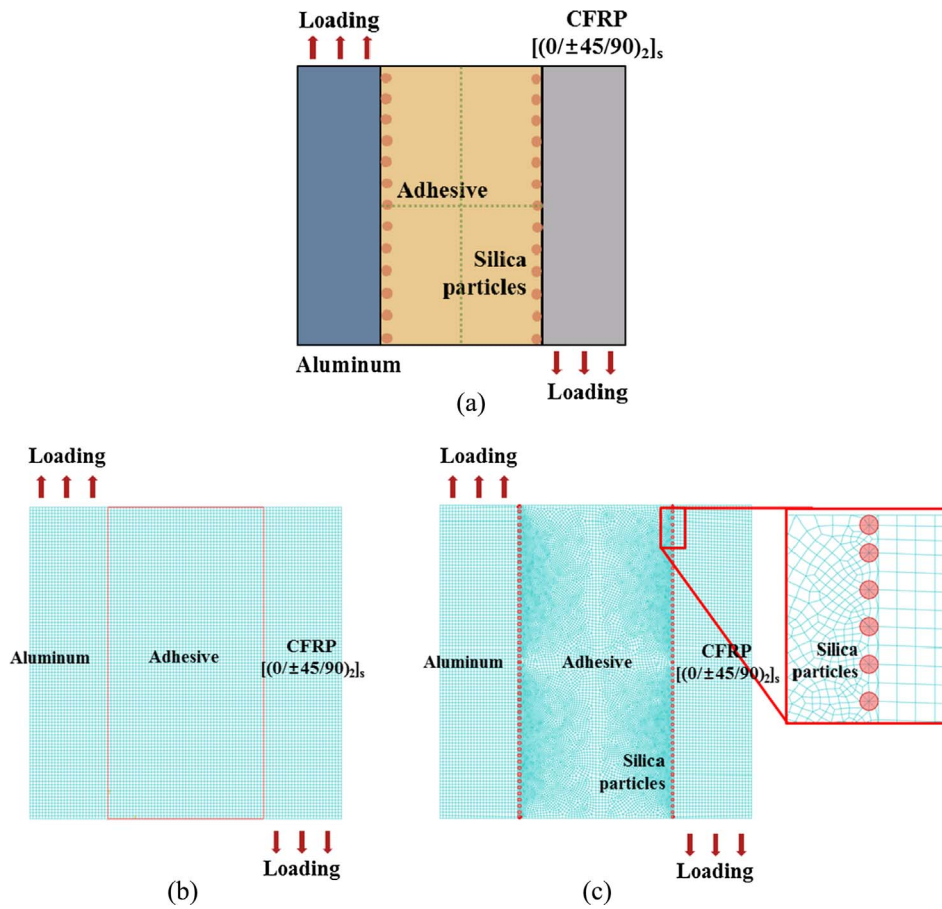
Fig. 2. (a) Schematic illustration of the simulation layout for lap shear test and the FE discretization of (b) bare and (c) silica-coated specimens.
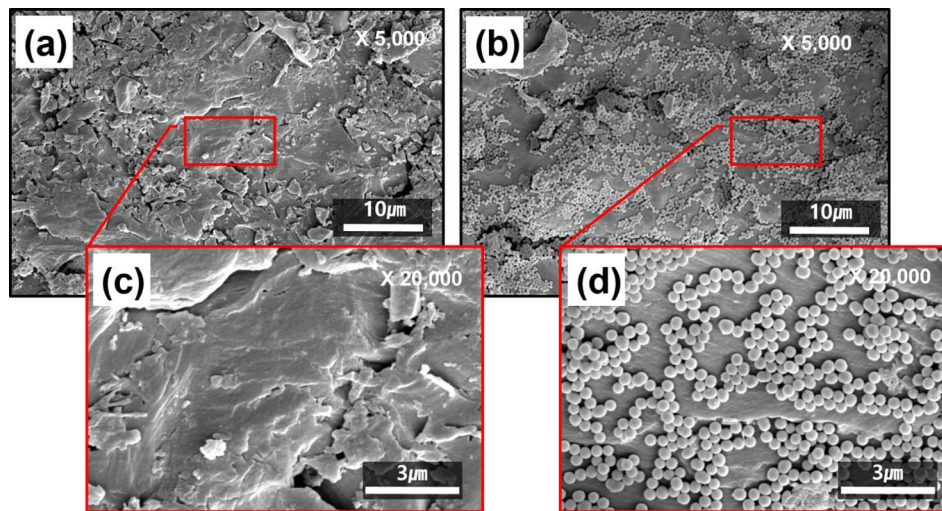

Fig. 3. FE-SEM images of bare CFRP surfaces with magnitudes of (a)5,000×, and (c)20,000×, and a silica-coated CFRP surface with a magnitude of (b)5,000×, (d)20,000×.

carbon fibers [31–33]. Both methods incur unnecessary environmental and economic costs, becoming one of the major obstacles to the industrial application of CFRP composites. In this respect, the ideal adhesive should strongly bond CFRP composites with other materials while at the same time should not damage the CFRP when debonding such that the detached composite parts retain their original conditions with the potential for reuse as well. Most studies thus far have focused on improvements of the adhesion force, whereas very few have been
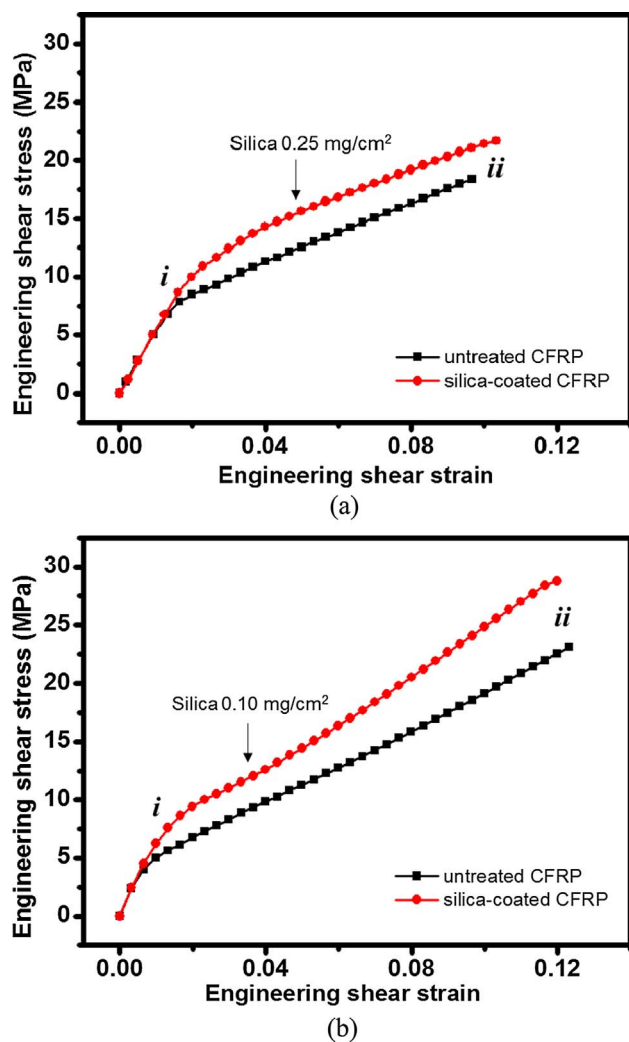
Fig. 4. Stress-strain curves of the lap shear test for (a) the Araldite 2011-A/B (paste type) adhesive and (b) the LF-501 (film type) adhesive. Black indicates bare CFRP while red represents silica-coated CFRP with the silica concentration of $0.25 \, \text{mg/cm}^2$ (a) and $0.10 \, \text{mg/cm}^2$ (b). *i.* yield stress, and *ii.* fracture stress.

carried out in an effort to minimize composite damage during the de-bonding step.

In this study, a CFRP composite was initially coated with silica particles via a simple dropping method, and an epoxy adhesive was applied to bond the CFRP to Al. A lap shear test was conducted to measure and analyze the mechanical properties, and a post-analysis step was done with optical microscopy and field-emission scanning electron microscopy (FE-SEM). A finite element (FE)-based theoretical analysis was also carried out to examine the interfacial characteristics of the adhesive, silica particles, and resulting CFRP/Al coupons. It was found that damage to the CFRP typically caused during debonding was significantly reduced by the introduction of the silica coating, showing the possibility of the reuse of CFRP composite materials. This is a unique research result in that this silica coating not only enhances the adhesive strength by 20% but also acts as a protection barrier to reduce CFRP composite damage during the debonding step. This will contribute to the development of an economical and environmentally friendly CFRP reuse system.

2. Methods

2.1. Materials

The adhesives used in this study were two different types of epoxy systems: Araldite 2011-A/B (paste type, Huntsman Co.) and LF-501 (film type, L&L Co.). 2 mm thick sheets of T-700 grade $[(0/\pm 45/90)_2]_S$ CFRP (C-ASK Co., Ltd.) and high-strength 2024T-4 Al (S.T. Co.) were purchased and cut into desired dimensions (12.5 mm wide and 50.5 mm long) using a water jet (TOPS Co., Ltd.). Silica particles with a diameter of 200–400 nm (Ditto Technology Co., Ltd.) and N,N-dimethyl for-mamide (DMF, Sigma Aldrich) were used to coat the surfaces of the CFRP composites and to disperse the silica particles properly, respectively [34–37]. Acetone was purchased from Daejung Chemical Co., Ltd. All chemicals were used as received without any additional pur-ification processes.

2.2. Fabrication of silica-coated CFRP/Al specimen

In order to determine the effect of the silica coating on the adhesive strength and failure behaviors, a silica-coated CFRP/Al lap shear spe-cimen was fabricated following the ASTM D 5868 standard. The de-tailed fabrication procedure is shown in Fig. 1, and it proceeded as follows: (i) the adhesion areas of the CFRP and Al coupons were first roughened with sandpaper to maximize the physical surface area and to adsorb silica particles more efficiently. The treated coupons were thoroughly cleaned with acetone and dried in an oven. (ii) Subse-quently, silica particles were dispersed in a solvent of DMF and soni-cated to produce a uniform colloidal solution [38]. Ultrasonic pulver-ization of 5–10 min was conducted, and various concentrations were prepared to determine the optimal silica concentration. The prepared colloidal silica solution was applied to the CFRP and Al adhesion area, where 8 μl of the 1–6% (w/v) silica colloidal solution was dropped onto an adhesion area of $12.5 \, \text{mm} \times 12.5 \, \text{mm}$ in size to make the con-centration of silica particles 0.05–$0.3 \, \text{mg/cm}^2$.

The DMF solvent was allowed to evaporate slowly at room tem-perature for 30 min. (iii) Two typical types of epoxy adhesives, Araldite 2011-A/B as a paste type and LF-501 as a film type, were applied to the silica-coated surfaces according to the manufacturer instructions such that the final thickness was approximately 0.1–0.2 mm to realize best adhesive performance. (iv) With the lap shear specimen fixed with a clamp, a curing procedure was performed inside a convection oven, where the temperature profile is summarized in detail in Table 2. (v) Finally, sandpapers were attached at both ends of the lap shear spe-cimen to prevent any possible slippage during the specimen extension process. The dimensions of the lap shear specimen is represented in Fig. 1.

2.3. Adhesive strength measurements and CFRP fracture observations

The tensile stress-strain measurements were performed using an Instron 5567A universal testing machine (UTM) following the ASTM D 5868 specification, where the lap shear specimen was a thin epoxy adhesive cured between rectangular CFRP and Al coupons. The cross-head displacement was 5 mm/min and the adhesive stress was de-termined from the ultimate strength value of the stress-strain curve. A fractographic study was conducted using a Nova nanoSEM-450 device (FEI Co.) in order to ascertain the effect of the silica coating on the failure mode. The CFRP fracture area was defined and calculated as the amount of fractured CFRP residue on the Al side surface after the lap shear test.
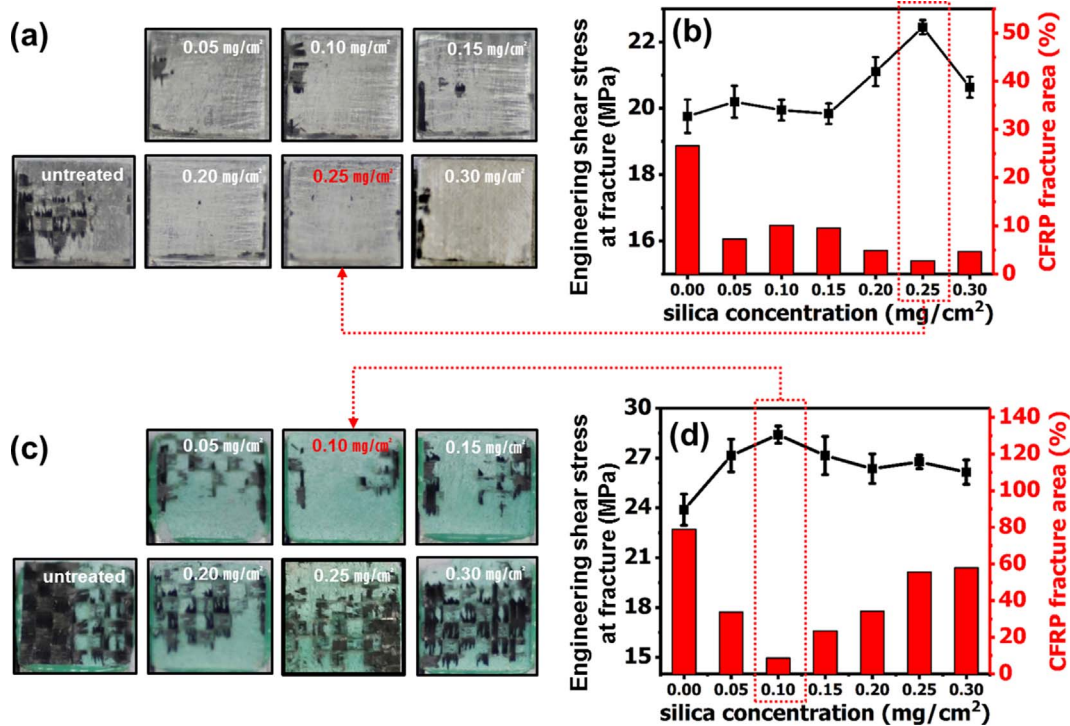
Fig. 5. Engineering shear stress at fracture and CFRP fracture area depending on the silica concentration: (a) and (c) show images of fractured surfaces on the Al side after the lap shear test, where the black areas represent fractured CFRP on the gray (or green) epoxy adhesive; (b) and (d) show the adhesive strength and CFRP fracture area plotted versus the silica concentration. (a) and (b) depict the results with the Araldite 2011-A/B adhesive and (c) and (d) indicate those with the LF-501 adhesive. The maximum adhesive strength with the minimum CFRP fracture is obtained with silica concentrations of 0.25 mg/cm² and 0.10 mg/cm² for Araldite 2011-A/B and LF-501, respectively.

2.4. Numerical simulations

A series of numerical simulations based on the FE method were carried out for a theoretical analysis and for a correlation with experimental observations. From the results of the lap shear test, our hypothesis was established and its mechanisms were assessed by a fractographic study via a FE-SEM analysis and CFRP fracture area calculations. However, it is difficult to conclude that a quantitative evaluation of the role of the silica particles on the CFRP surface was satisfactorily described. To overcome this, FE modeling was conducted here, as shown in Fig. 2. A different approach from an experiment, such as a numerical analysis, of the same phenomena is expected to provide better insight into the experimental observations.

The lap shear test was reconstructed in a simplified form for efficiency of the simulation, as shown in Fig. 2a, where the Al coupon was placed on the left side and the CFRP in $[(0/\pm 45/90)_2]_s$ on the right side with silica particles placed on the surface of each coupon. Loading was applied to the top direction of Al and to the bottom of the CFRP coupon such that it would induce shear deformation on the epoxy adhesive. It should be noted that the silica particles are assumed to be a rigid body in the present simulation in that the strength of the silica particles is much higher than that of the adhesive [39]. The constructed FE 3D models of the bare and silica-coated specimens are shown in Fig. 2b and c, respectively. The generated models consist of 20,000–25,000 elements, and the meshes are arranged densely on the silica particle side to improve the calculation accuracy.

The material properties for Al and CFRP were chosen in accordance with reference values, as follows: $E_{Al} = 68$ GPa, $\nu_{Al} = 0.347$; $E_{CFRP} = 148$ GPa, and $\nu_{CFRP} = 0.300$, where E and ν denote the Young'

modulus and Poisson's ratio, respectively [40–42]. The lap shear behaviors of the specimens were described through a calibration method based on an elastic-plastic model, which is an approach built into ABAQUS [43,44]. The elastic moduli and plastic parameters utilized in the present simulations are, therefore, estimated from the calibration of the stress-strain behaviors of the specimens. The failure criterion was also determined based on the experimentally measured stress-strain curves.

3. Results and discussion

3.1. FE-SEM images of bare and silica-coated CFRP surfaces

The shape, size and dispersion of the silica particles coated onto the CFRP surfaces were examined using FE-SEM, as presented in Fig. 3, where Fig. 3a and b show the surfaces of the bare CFRP and silica-coated CFRP samples, respectively. Fig. 3c and d are magnified images of Fig. 3a and b. As expected, a major difference was noted between the bare and silica-coated CFRP surfaces. With the silica coating, spherically shaped silica particles were observed to be uniformly distributed on the surface of the CFRP (Fig. 3b and d), whereas no such particles were found on the bare CFRP surface (Fig. 3a and c). Furthermore, at the optimal concentration, the silica particles are well dispersed on the CFRP surfaces as a single layer without aggregation. The average diameter of the spherical silica particles as measured from the SEM images was found to be around 320 nm, which is in the range of the manufacturer's specifications (Ditto Technology Co., Ltd.). It is noteworthy that the strength at which the silica particles adsorbed onto the CFRP surfaces was strong such that they did not come off under ultra-
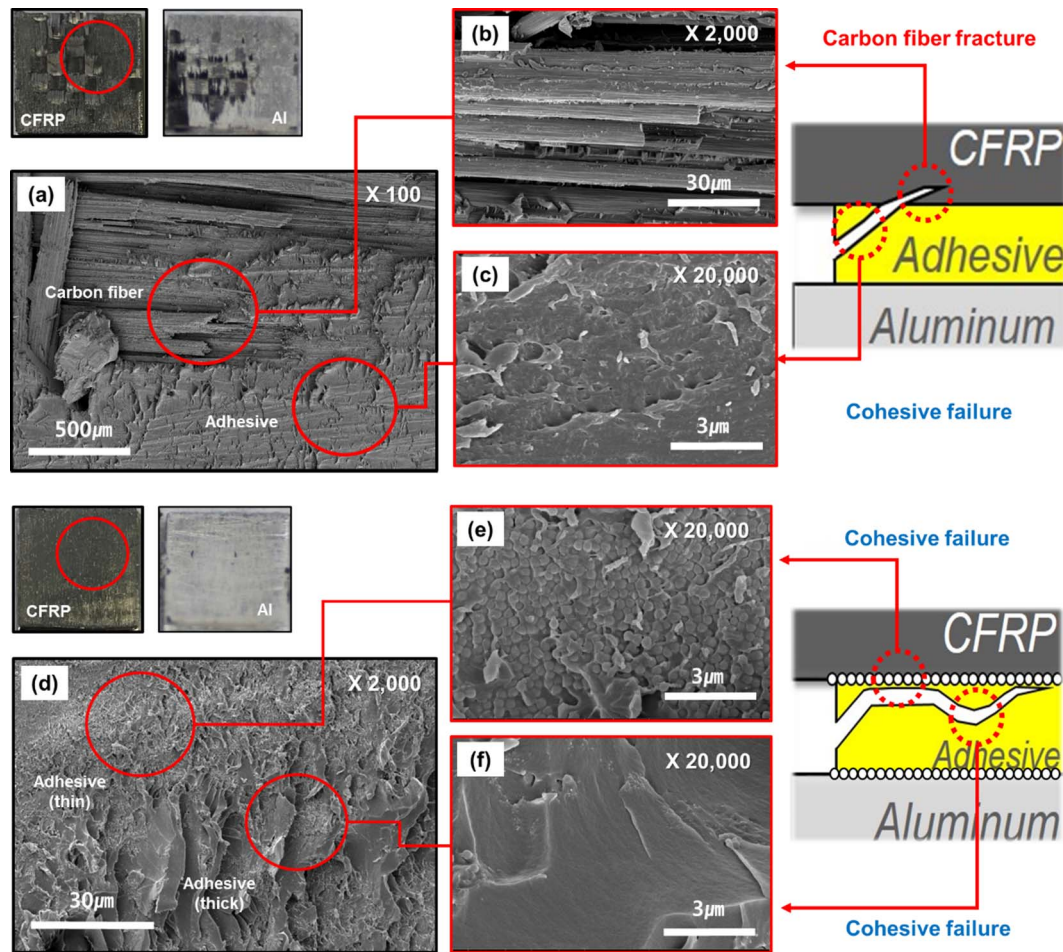
Fig. 6. FE-SEM images of fractured surfaces on the CFRP side after the lap shear test for (a), (b), and (c) bare CFRP, and (d), (e), and (f) silica-coated CFRP. (b) and (c) are enlarged images of (a), where carbon fibers and polymer are observed, respectively. (e) and (f) are enlarged images of (d), where silica layers and epoxy adhesive are correspondingly shown. The schematics on the right indicate how the fracture propagates based on FE-SEM images.

sonication conditions for an extended period of time.

3.2. Stress-strain behaviors

For lap shear specimens with two different types of epoxy adhesives, the stress versus strain measurements were taken at a crosshead displacement speed of 5 mm/min, as shown in Fig. 4. Fig. 4a and b correspondingly present the stress-strain behaviors for the Araldite 2011-A/B and LF-501 epoxy adhesives with the black and red colors each indicating the bare and silica-coated specimens. It is noted that the amounts of silica applied were 0.25 mg/cm^2 for Araldite 2011-A/B and 0.10 mg/cm^2 for LF-501. Examining the stress–strain curves shown in Fig. 4, the stress-strain curves during shear deformation display three distinct regimes: (i) an initial linear region at small strains, (ii) a bending region corresponding to the yield where the epoxy adhesives begin to flow (Fig. 4i), and (iii) a second linear region with a reduced slope indicating that the epoxy adhesive becomes less stiff. As deformation continues, the lap shear specimen undergoes a final fracture, as indicated in Fig. 4ii.

Araldite 2011-A/B displays higher yield stress but lower failure stress than LF-501, and it is well understood in that every epoxy system

has different thermal and mechanical properties. Of particular interest is the effect of the silica coating on the stress-strain behaviors. As clearly observable in Fig. 4, when silica was coated onto the CFRP surface, both the yield and failure stresses increase by around 20% (18.4–21.7 MPa for Araldite 2011-A/B and 23.1–28.8 MPa for LF-501). This enhancement in the yield and failure stress has been reported when silica particles are embedded into bulk epoxy and is usually attributed to a longer crack path or the silica-induced yield phenomenon [45–47]. However, in this study, a similar effect was achieved only with a surface coating. None of the above explanations can be applied to explain the increases in the yields or failure stress levels of the silica-coated CFRP, and this could not be clarified at this point.

3.3. Dependence of the adhesive strength and CFRP fracture area on the silica concentration

The adhesive strength is defined as the value at which a lap shear specimen fails, and its dependence on the silica concentration was investigated here. Stress-strain measurements were repeated on a series of lap shear specimens with different silica concentrations of 0.05, 0.1, 0.15, 0.2, 0.25 and 0.3 mg/cm^2, during which unexpected findings
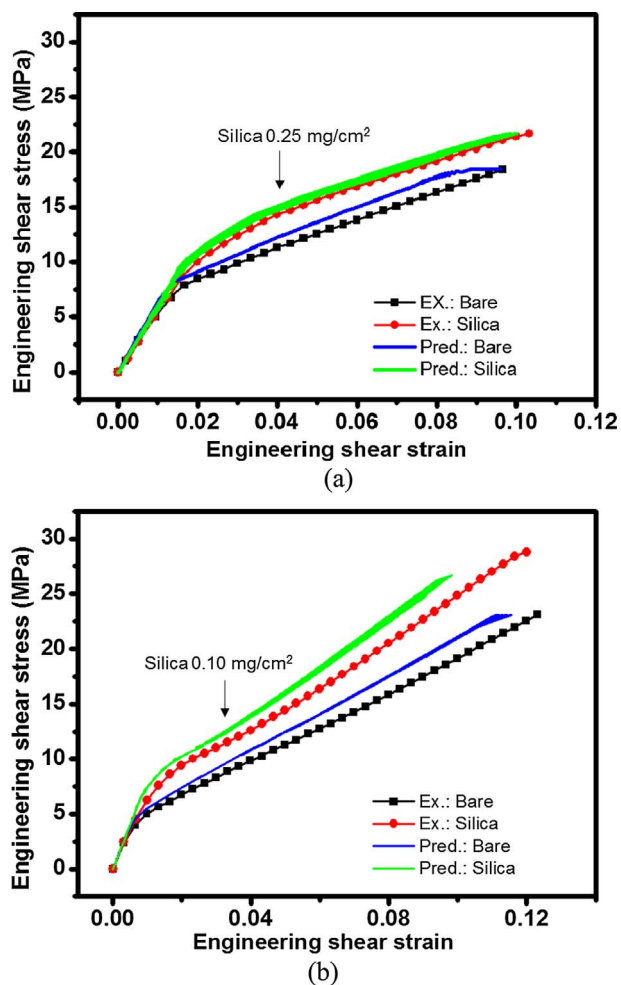
Fig. 7. Experimental comparisons with the present numerical analysis of (a) Araldite 2011-A/B and (b) LF-501 adhesives. The silica concentrations of 0.25 mg/cm² and 0.10 mg/cm² were applied for (a) and (b), respectively.

were discovered in that the fracturing of CFRPs which occurs during the failure of a lap shear specimen is significantly decreased with the silica coating. Therefore, the adhesive strength and CFRP fracture area were plotted versus the silica concentration, as shown in Fig. 5b and d, where the black line corresponds to the adhesive strength (left axis) and the red column corresponds to the CFRP fracture area (right axis). Here, the CFRP fracture area was defined as the fractured portions of the CFRP as quantified from the amount of fractured CFRP residue on the surface of the Al coupon, as indicated in Fig. 5a and c.

Very interestingly, as can be seen in Fig. 5b and d, the maximum adhesive strength was attained when the CFRP fracture areas were at the minimum levels. Moreover, this holds for the two typical types of epoxy adhesives tested here, i.e., Araldite 2011-A/B and LF-501. For example, the adhesive strength for the paste-type adhesive (Araldite 2011-A/B) at a silica concentration of 0.25 mg/cm² was 21.7 MPa, which is 17.8% higher than that of a bare specimen (18.4 MPa). On the other hand, the CFRP fracture areas for the bare and silica-coated CFRPs were respectively 26.6% and 2.7%, representing an improvement of 89.3% in damage reduction by the simple silica coating method. Similar results were obtained for the film-type adhesive of LF-

501. The adhesive strength increased by 24.6% from 23.1 to 28.8 MPa and the fracture area decreased by 89% from 79.0 to 8.8% at a silica concentration of 0.10 mg/cm².

As the silica concentration increased, the adhesive strength is enhanced and the CFRP fracture area diminishes until the optimum concentration is reached. Past the optimum concentration, the adhesive strength starts to decrease and the CFRP fracture area increases. It appears that the application of excess silica causes serious aggregation, inducing poor surface conditions and degradation of the adhesive performance. Both the paste and film types of epoxy adhesives display the same tendency: a reduction of the CFRP fracture area and an increase in the adhesive strength at the optimal silica concentration as compared to bare CFRP. It was unexpectedly discovered that the adhesive strength and CFRP fracture area were inversely proportional to each other.

Recent requirements for adhesives on CFRP composites include not only increased adhesive strength but also decreased material damage in order to reuse expensive composite parts. However, enhanced adhesive strength has generally caused CFRP damage during debonding; thus, this conflict has so far been technically challenging despite its great importance in relation to practical applications of adhesives. By applying the proposed method, the CFRP fracture was significantly reduced by around 90% even with the increase of the adhesive strength by about 20%. To the best of our knowledge, this is the first study of adhesives to address the adhesive strength and damage protection simultaneously. Moreover, it is believed that the findings here will contribute to the substantial growth in the use of adhesives and/or to the CFRP reuse market.

3.4. Fractographic study on Silica-Coated CFRP composites

In order to examine the effects of silica particles coated onto coupon surfaces, a post-analysis was conducted after the failure of the lap shear sample. FE-SEM images of the fractured surfaces on the CFRP side are shown in Fig. 6. The fractured surfaces of the bare and silica-coated specimens are correspondingly displayed in Fig. 6a–f. For the bare specimen, some parts of the carbon fibers and matrix were torn off such that the carbon fibers initially embedded inside the adhesive ended up being exposed to the fractured surface, as shown in Fig. 6a and b. On the other hand, when the silica particle coating was applied to each coupon surface, no carbon fibers and only the adhesive layer could be observed, with some variations in the thickness. It is interesting to note that some epoxy adhesive remained in the form of such a thin layer that the silica coating beneath could clearly be observed, as shown in Fig. 6e.

Examining the FE-SEM images in Fig. 6, the bare CFRP was fractured in two different ways, i.e., a CFRP fracture and an adhesive fracture, while the silica-coated CFRP showed only an adhesive fracture. It is plausible to consider that direct damage to the CFRP itself may have caused a decrease in the adhesive strength in the bare CFRP lap shear test, representing a serious obstacle preventing CFRP reuse. On the other hand, for the silica-coated specimen, it appears that the surfaces coated with silica particles acted as a physical protection barrier such that the silica layer actually prevented cracks from propagating into the CFRP. The right side of Fig. 6 shows schematics that describe the effect of the silica coating on the CFRP and Al, where cracks occurred at both adhesives and at the CFRP for the bare specimen, whereas cracks arose at only the adhesive in the other case due to the protection of the coated silica barrier layer.
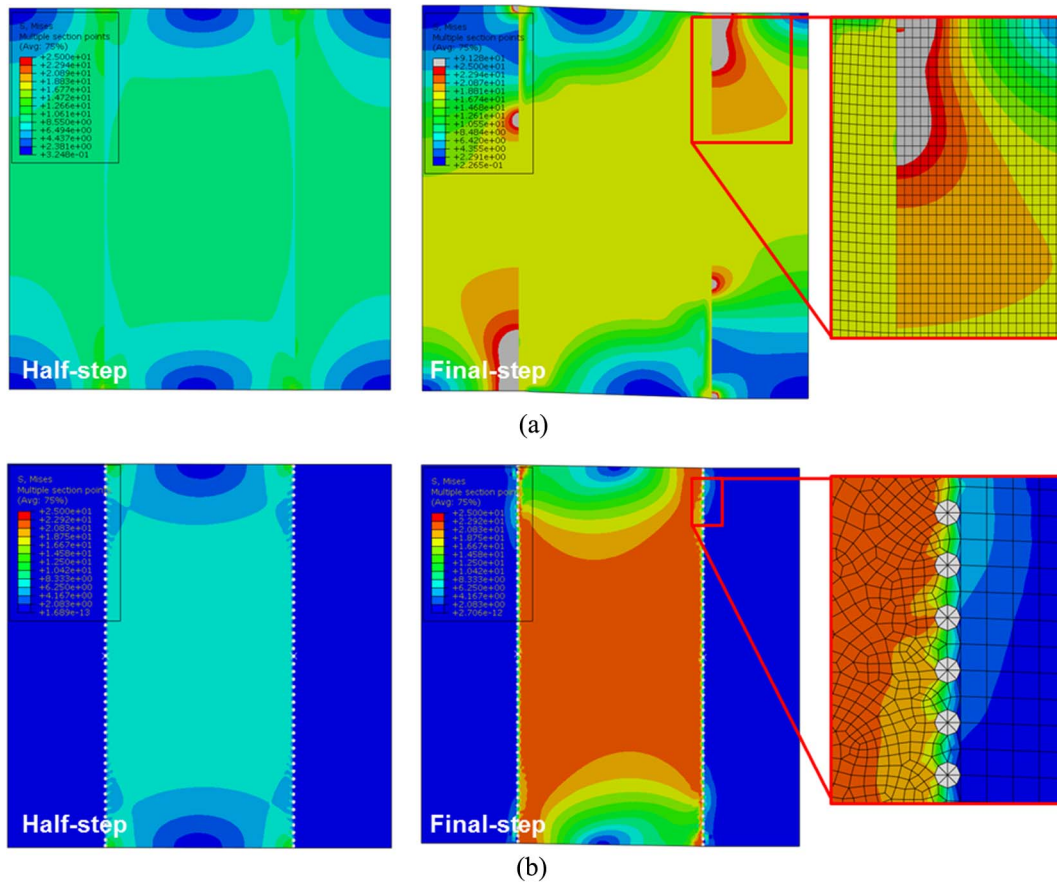
Fig. 8. Representative von-Mises stress distributions of (a) bare and (b) silica-coated specimens with different simulation steps.

3.5. Numerical analysis

The stress-strain responses of the bare and silica-coated specimens were compared under identical loading and boundary conditions, as shown in Fig. 7. With only a slight discrepancy, the predicted lap shear responses were in good agreement with the experimental results. The main reason for this difference may have been the simplified model used here for improved simulation efficiency. It is also believed that the differences may stem from the assumption of complete bonding between the silica particles and the CFRP/Al components, while actual silica particles on the surfaces of CFRP and Al are probabilistically debonded and agglomerated rather than completely bonded and uniformly distributed. More accurate predictions would be made when the above items are reflected in the present simulation; however, these phenomena are difficult to consider through a FE-based numerical approach. Because the interfacial properties between the silica particles and CFRP/Al components are currently outside the scope of this study, this aspect is not considered in this paper, though it can be further developed in the future.

The representative von-Mises stress distributions of the bare and silica-coated lap shear specimens with different simulations step are shown correspondingly in Fig. 8a and b. For the bare specimen, the simulation predicted that the von-Mises stress distributions on and inside the CFRP and Al components would be considerable. On the other hand, for the silica-coated specimen, the stress levels were mainly concentrated on the silica surfaces coated onto the CFRP and Al components. The reason for this prediction can be deduced by considering the enlarged image shown in Fig. 8b. The silica particles coated onto the coupons serve as a barrier, preventing the stress from propagating into the CFRP or Al components. These simulation results are consistent with the SEM analysis outcomes and the fractographic schematics illustrated in Fig. 6. The silica particles cause fractures to occur inside the adhesive or at the periphery of the silica particles such that the failure occurs on top of the silica coatings instead of in the attached materials.

For a further analysis, the reaction force with identical specimens and boundary conditions was calculated, as shown in Fig. 9. The reaction force is the level of resistance against movement by an external load or deformation, and it may address the influence of the silica particle coating in the lap shear test. As shown in Fig. 9, the distributions of the reaction forces at the interfaces of the adhesive and the CFRP/Al components are substantially different; for the bare specimen, the reaction force is noted both along the interface and inside the attached materials (Fig. 9a). However, for the silica-coated lap shear specimen, a saw-tooth pattern is observed and the reaction force is highly concentrated near the silica-particle coating layer (Fig. 9b). It is presumed that the silica coating on the surface of the specimens manifests an interlocking mechanism, which represents a possible explanation of the improved responses in the lap shear test.
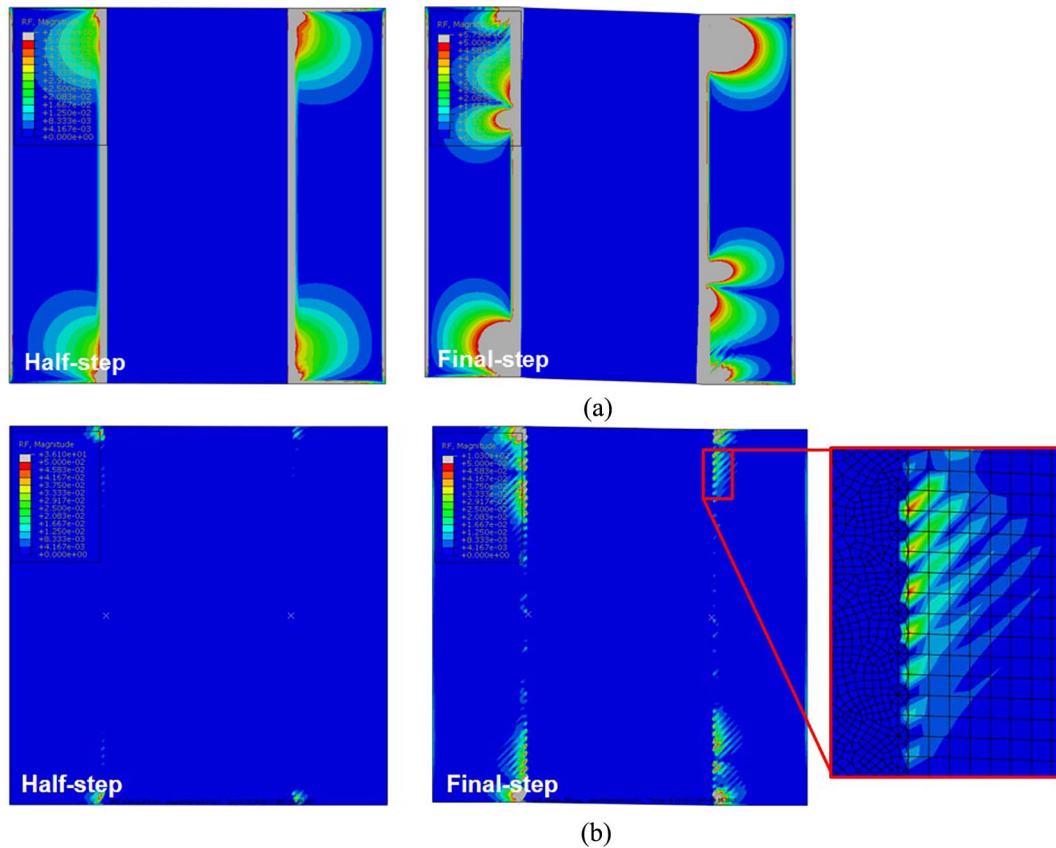
(a)

(b)

Fig. 9. Representative reaction force distributions of (a) bare and (b) silica-coated specimens.

4. Conclusions

The present study focused on the development of a novel means of silica coating of CFRP composites to improve the adhesive strength while at the same time significantly reducing CFRP fracturing during the debonding process. Silica particles were coated in the form of a well-dispersed monolayer by a simple coating method using silica colloids in DMF without complicated chemical and/or electrochemical treatments. Unlike previous publications in which silica particles were embedded into a bulk adhesive and only an adhesion improvement was observed, in this study the silica coating layer was applied onto the surface of CFRP to protect the substrates and improve the adhesive force simultaneously. The coating approach with silica particles proposed in this study is quite promising considering the performance improvement it offers as well as the superior damage protection and convenience of application compared to conventional methods. The following three main conclusions can be drawn from the research results.

- A simple method for a uniformly distributed single silica-particle coating layer was developed.
- The proposed particle coating significantly reduces the fractures of CFRP composites during debonding while at the same time improving the adhesive strength.
- The optimum concentration of silica particles differs depending on the adhesive types. It was also predicted that the optimum concentration would vary in accordance with the particle type used, i.e., rubber, platinum, silver, etc.

Additional experimental parameters, including the particle size, surface treatment, and curing method, should be considered for a clear understanding of the physio-chemical mechanisms in this study. This would be beyond the scope of the paper. Nonetheless, we plan to extend our work along this direction in the near future.

References

[1] Heuss R, Müller N, van Sintern W, Starke A, Tschiesner A. Lightweight, heavy impact. Hg v McKinsey McKinsey. 2012.
[2] Hale J. Boeing 787 from the ground up. Aero 2006;4(24):7.
[3] Fawcett AJ, Oakes GD. Boeing composite airframe damage tolerance and service experience. Composite Damage Tolerance & Maintenance Workshop 2006.
[4] Shama Rao N, Simha T, Rao K, Ravi Kumar G. Carbon composites are becoming competitive and cost effective. White paper from www infosys com. 2014.
[5] Zhu J-T, Wang X-L, Kang X-D, Li K. Analysis of interfacial bonding characteristics of CFRP-concrete under fatigue loading. Constr Build Mater 2016;126:823–33.
[6] Huang Z, Sugiyama S, Yanagimoto J. Hybrid joining process for carbon fiber reinforced thermosetting plastic and metallic thin sheets by chemical bonding and plastic deformation. J Mater Process Technol 2013;213(11):1864–74.
[7] Park HM, Kim G, Lee SY, Jeon H, Kim SY, Kim M, et al. Electrical resistivity reduction with pitch-based carbon fiber into multi-walled carbon nanotube (MWCNT)-embedded cement composites. Constr Build Mater 2018;165:484–93.
[8] Ataş A, Soutis C. Application of cohesive zone elements in damage analysis of composites: strength prediction of a single-bolted joint in CFRP laminates. Int J Non Linear Mech 2014;66:96–104.
[9] Matsuzaki R, Shibata M, Todoroki A. Improving performance of GFRP/aluminum single lap joints using bolted/co-cured hybrid method. Compos A Appl Sci Manuf 2008;39(2):154–63.
[10] Malinowski PH, Wandowski T, Ostachowicz WM. Characterisation of CFRP adhesive bonds by electromechanical impedance. In: SPIE smart structures and materials + nondestructive evaluation and health monitoring. International Society for Optics and Photonics; 2014. p. 906415–7.
[11] Chen L, Chai S, Liu K, Ning N, Gao J, Liu Q, et al. Enhanced epoxy/silica composites mechanical properties by introducing graphene oxide to the interface. ACS Appl Mater Interfaces 2012;4(8):4398–404.

[12] Yang S, Choi J, Cho M. Elastic stiffness and filler size effect of covalently grafted nano-silica polyimide composites: molecular dynamics study. ACS Appl Mater Interfaces 2012;4(9):4792–9.

[13] Yoonessi M, Lebrón-Colón M, Scheiman D, Meador MA. Carbon nanotube epoxy nano-composites: the effects of interfacial modifications on the dynamic mechanical properties of the nanocomposites. ACS Appl Mater Interfaces 2014;6(19):16621–30.

[14] Souri H, Yu J, Jeon H, Kim JW, Yang C-M, You N-H, et al. A theoretical study on the piezoresistive response of carbon nanotubes embedded in polymer nanocomposites in an elastic region. Carbon 2017;120:427–37.

[15] Korayem AH, Chen SJ, Zhang QH, Li CY, Zhao XL, Duan WH. Failure of CFRP-to-steel double strap joint bonded using carbon nanotubes modified epoxy adhesive at moderately elevated temperatures. Compos B Eng 2016;94:95–101.

[16] Korayem AH, Li CY, Zhang QH, Zhao XL, Duan WH. Effect of carbon nanotube modified epoxy adhesive on CFRP-to-steel interface. Compos B Eng 2015;79:95–104.

[17] Lionetto F, Frigione M. Environmental effects on the adhesion properties of nanos-tructured epoxy-silica hybrids. J Appl Polym Sci 2015;132(36).

[18] Reitz V, Meinhard D, Ruck S, Riegel H, Knoblauch V. A comparison of IR-and UV-laser pretreatment to increase the bonding strength of adhesively joined aluminum/CFRP components. Compos A Appl Sci Manuf 2017;96:18–27.

[19] Blass D, Kreling S, Nyga S, Westphalen T, Jungbluth B, Hoffman H-D, et al. CFRP bonding pre-treatment with laser radiation of 3 μm wavelength: laser/material interaction. SPIE LASE: International Society for Optics and Photonics; 2016. p. 973614–11.

[20] Yokozeki T, Ishibashi M, Kobayashi Y, Shamoto H, Iwahori Y. Evaluation of adhesively bonded joint strength of CFRP with laser treatment. Adv Compos Mater 2016;25(4):317–27.

[21] Palmieri FL, Belcher MA, Wohl CJ, Blohowiak KY, Connell JW. Laser ablation surface preparation for adhesive bonding of carbon fiber reinforced epoxy composites. Int J Adhes Adhes 2016;68:95–101.

[22] Sánchez Serrano J, Ureña A, Lazcano Ureña S, Blanco Varela T. New approach to surface preparation for adhesive bonding of aeronautical composites: atmospheric pressure plasma. Studies on the pretreatment lifetime and durability of the bondline. Compos Interfaces 2015;22(8):731–42.

[23] Okada T, Kanda M, Faudree MC, Nishi Y. Shear strength of adhesive lamination joint of aluminum and CFRP sheets treated by homogeneous low energy electron beam irradia-tion prior to lamination assembly and hot-press. Mater Trans 2014;55(10):1587–90.

[24] Wang H, Hao X, Zhou H, Li D, Hua L. Study on ultrasonic vibration-assisted adhesive bonding of CFRP joints. J Adhes Sci Technol 2016;30(17):1842–57.

[25] Batuwitage C, Fawzia S, Thambiratnam D, Al-Mahaidi R. Durability of CFRP strengthened steel plate double-strap joints in accelerated corrosion environments. Compos Struct 2017;160:1287–98.

[26] Park S, Yang B, Kim B, Ha S, Lee H. Structural strengthening and damage behaviors of hybrid sprayed fiber-reinforced polymer composites containing carbon fiber cores. Int J Damage Mech 2017;26(2):358–76.

[27] Jeon H, Yu J, Lee H, Kim G, Kim JW, Jung YC, et al. A combined analytical formulation and genetic algorithm to analyze the nonlinear damage responses of continuous fiber toughened composites. Comput Mech 2017;60(3):393–408.

[28] Yang B, Ha S, Pyo S, Lee H. Mechanical characteristics and strengthening effectiveness of random-chopped FRP composites containing air voids. Compos B Eng 2014;62:159–66.

[29] Job S. Composite recycling: summary of recent research and development. Materials KTN Report. 2010:26–42.

[30] Yazdanbakhsh A, Bank LC. A critical review of research on reuse of mechanically recycled FRP production and end-of-life waste for construction. Polymers 2014;6(6):1810–26.

[31] Limburg M, Quicker P. Disposal of carbon fiber reinforced polymers. Wind Energy 6(7):14.

[32] Prinçaud M, Aymonier C, Loppinet-Serani A, Perry N, Sonnemann G. Environmental feasibility of the recycling of carbon fibers from cfrps by solvolysis using supercritical water. ACS Sustain Chem Eng 2014;2(6):1498–502.

[33] Okajima I, Hiramatsu M, Shimamura Y, Awaya T, Sako T. Chemical recycling of carbon fiber reinforced plastic using supercritical methanol. J Supercrit fluids 2014;91:68–76.

[34] Li J, Ye F, Vaziri S, Muhammed M, Lemme MC, Östling M. A simple route towards high-concentration surfactant-free graphene dispersions. Carbon 2012;50(8):3113–6.

[35] Cheng Q. Dispersion of single-walled carbon nanotubes in organic solvents. Dublin: Dublin Institute of Technology; 2010.

[36] Zhao S, Yan W, Shi M, Wang Z, Wang J, Wang S. Improving permeability and antifouling performance of polyethersulfone ultrafiltration membrane by incorporation of ZnO-DMF dispersion containing nano-ZnO and polyvinylpyrrolidone. J Membr Sci 2015;478:105–16.

[37] Wu L, Huang Y, Liu L, Meng L. Interaction and stabilization of DMF-based alumina sus-pensions with citric acid. Powder Technol 2010;203(3):477–81.

[38] Caneba G, Dutta C, Agrawal V, Rao M. Novel ultrasonic dispersion of carbon nanotubes. J Miner Mater Character Eng. 2010;9(03):165.

[39] Yang B, Na S, Jang J, Kim H, Lee H. Thermo-mechanical analysis of road structures used in the on-line electric vehicle system. Struct Eng Mech 2015;53(3):519–36.

[40] Oliver WC, Pharr GM. An improved technique for determining hardness and elastic modulus using load and displacement sensing indentation experiments. J Mater Res 1992;7(06):1564–83.

[41] Herakovich CT. Mechanics of fibrous composites. New York: John Wiley & Sons Inc; 1998. p. 1998.

[42] Simmons G, Wang H. Single crystal elastic constants and calculated aggregate properties. 1971.

[43] Hibbett, Karlsson, Sorensen. ABAQUS/standard: user's manual. Hibbitt, Karlsson & Sorensen; 1998.

[44] Kim SY, Jang HG, Yang C-M, Yang B. Multiscale prediction of thermal conductivity for nanocomposites containing crumpled carbon nanofillers with interfacial characteristics. Compos Sci Technol 2018;155:169–76.

[45] Ma P, Jiang G, Li Y, Zhong W. The impact compression behaviors of silica nanoparti-cles—epoxy composites. J Textile Sci Technol 2015;1(01):1.

[46] Ma H-L, Jia Z, Lau K-T, Li X, Hui D, Shi S-Q. Enhancement on mechanical strength of adhesively-bonded composite lap joints at cryogenic environment using coiled carbon nanotubes. Compos B Eng 2017;110:396–401.

[47] Hosur M, Barua R, Zainuddin S, Jeelani S, Kumar A, Trovillion J, et al. Processing and characterization of epoxy nanocomposites with Mwcnt's/Cnf's using thinky and 3-roll shear mixing techniques. Matéria (Rio de Janeiro) 2010;15(2):247–53.